Input-Output Feedback Linearization Control of a Linear Induction Motor Taking into Consideration its Dynamic End-effects and Iron Losses

Angelo Accetta[a], Maurizio Cirrincione[b], Filippo D'Ippolito[c], Marcello Pucci[a], Antonino Sferlazza[c]

[a]INstitute for Marine engineering (*INM*), section of Palermo, National Research Council of Italy (*CNR*), Via Ugo La Malfa 153, 90146 Palermo, Italy. (angelo.accetta@cnr.it, marcello.pucci@cnr.it)
[b]School of Engineering, University of the South Pacific, Laucala Campus, Suva, Fiji Islands. (m.cirrincione@ieee.org)
[c]Department of Engineering (*DI*), University of Palermo, viale delle scienze Ed. 10, 90128 Palermo, Italy. (filippo.dippolito@unipa.it, antonino.sferlazza@unipa.it)

***Abstract*— This paper proposes a new input-output feedback linearization control technique (*FLC*) of Linear Inductions Motors (*LIMs*) taking into consideration both the dynamic end-effects and the iron losses. Starting from a previously conceived dynamic model including both the dynamic end-effects and the iron losses, all the theoretical framework of the FLC has been developed. The proposed FLC improves a previously proposed version of FLC in accounting also the iron losses, which in LIMs with fixed secondary sheet play a much important role than in RIMs. The proposed FLC has been experimentally tested on a suitably developed test set-up.**

***Index Terms*—Linear Induction Motor (*LIM*), Input-output Feedback Linearization Control (*FLC*), Dynamic end-effects, Iron Losses, Space-vector State Model**

I. Introduction

Linear Induction Motors (*LIMs*) have been studied for several years [1]–[4] mainly because of their ability to develop a direct linear motion without the need of any rotating to linear motion transformation. Today, LIMs are more and more adopted in MAGLEV (Magnetically Levitation) vehicles, urban people movers, X-Y planar motion industrial platforms, launchers, actuators for industry and automotive. Nevertheless, their model is significantly more complex and presents more nonlinearities than the one of the rotating induction motor (*RIM*).This results in more involved control techniques than the ones adopted in RIMs. As for the dynamic models, the main issues are linked with the proper representation of the so-called end-effects, both static and dynamical, the latter being more important. On the basis of the knowledge of the geometrical and construction data of the LIM, [5] and [6] have developed dynamical models which consider both static and dynamical end-effects. Subsequently, [7] has proposed a model accounting for end-effects and transversal edge-effects by defining specific coefficients multiplying the electrical parameters of the LIM. More recently, [4], [8] have proposed a space-vector dynamic model of the LIM, taking into consideration the dynamic end-effects. This model has been expressed in a state form and afterwards successfully exploited for the development of non-linear control techniques adapted to LIMs [9]–[12], non-linear observers, and sensorless techniques [13], [14]. This model presents also the equation of the braking force due to the dynamic end-effects, expressed as a function of the chosen state variables. None of the above cited dynamic models, however, takes into consideration the iron losses of the LIM. Accounting for the iron losses is, in the LIM, even more significant than in the RIM, especially in case of LIMs with fixed secondary track. Indeed, in the RIM only the stator, which is laminated, is affected by the air-gap field rotating at the supply frequency. On the other hand, in the LIM the part affected by the air-gap field translating at frequency supply is the secondary, whose back iron is not laminated. In LIMs, therefore, differently from RIMs, iron losses are concentrated in the secondary track and cannot be neglected. Only recently has a dynamic model of the LIM been presented, accounting for both the dynamic end-effects and iron losses, expressed in state form [15]. To properly account for the iron losses, this model increases the number of electric state variables from 4 of the model in [8] to 6. This paper, starting from the dynamic model including both the dynamic end-effects and the iron losses, proposes a new input-output feedback linearization control (*FLC*) technique. This FLC inherently accounts for both effects and therefore improves the dynamic performance achievable with the previously presented FLCs [9]–[11]. The space-vector dynamic model of the LIM, on which the proposed FLC is based, has been presented in [15]. This model is particularly suitable for the application of the FL technique, since it is expressed in a state form. Starting from this dynamic space-vector model, a control system has been designed which, on the basis of the estimated secondary flux linkage and measured linear speed, provides two suitably defined additional control variables. The control system is designed in such a way that the adoption of these control variables corresponds to dealing with an equivalent LIM model which is linear and expressed in canonical control form. Finally, the real control variables of the machine, corresponding to the direct and quadrature components of the primary voltages expressed in the primary

978-1-7281-5826-6/20/$31.00 ©2020 IEEE

reference frame, are obtained from the additional ones by using a set of suitably defined non-linear functions, depending on both these additional control inputs and the LIM electric variables. The FLC has been assessed experimentally on a suitably developed experimental rig.

II. State space-vector model of the LIM including end-effects and the iron losses

This paper considers the space-vector electrical circuit of the LIM, including end effects and iron losses. This model was developed in [15] and, particularly, presents time-varying parameters to account for end effects and iron losses. This last feature was modelled with a transversal resistance R_0. Only the fundamentals of this model are presented here for the application of the FLC strategy, which is the main focus of the paper.

If the resistance R_0 accounting for the iron losses is to be considered, then the constraint linking together the currents in the 3 inductances is not valid any more. Consequently, the electrical state variables increase from 4 to 6. Considering that the iron losses depend on the three-phase magnetizing flux, the following set of state variables has to be chosen [15]:

$$\mathbf{x} = \begin{bmatrix} i_{sD} & i_{sQ} & \psi_{mD} & \psi_{mQ} & \psi_{rD} & \psi_{rQ} \end{bmatrix}. \tag{1}$$

Defining the space-vectors: $\mathbf{i}_s = i_{sD} + j i_{sQ}$, $\mathbf{\Psi}_m = \psi_{mD} + j\psi_{mQ}$, $\mathbf{\Psi}_r = \psi_{rD} + j\psi_{rQ}$ and $\mathbf{u}_s = u_{sD} + j u_{sQ}$, the complete state representation of the LIM, including both the dynamic end effects and the iron losses, can be written in compact form as follows:

$$\begin{bmatrix} \frac{d\mathbf{i}_s}{dt} \\ \frac{d\mathbf{\Psi}_m}{dt} \\ \frac{d\mathbf{\Psi}_r}{dt} \end{bmatrix} = \begin{bmatrix} \frac{R_0 - R_s}{L_{\sigma s}} & \frac{R_0 L_r}{\hat{L}_m L_{\sigma s} L_{\sigma r}} & \frac{-R_0}{L_{\sigma s} L_{\sigma r}} \\ R_0 & \frac{-R_0 L_r}{\hat{L}_m L_{\sigma r}} - \frac{\hat{R}_r}{\hat{L}_m} & \frac{R_0}{L_{\sigma r}} \\ 0 & \frac{R_r}{L_{\sigma r}} - \frac{\hat{R}_r}{\hat{L}_m} & j\omega_r - \frac{R_r}{L_{\sigma r}} \end{bmatrix} \begin{bmatrix} \mathbf{i}_s \\ \mathbf{\Psi}_m \\ \mathbf{\Psi}_r \end{bmatrix} + \begin{bmatrix} \frac{1}{L_{\sigma s}} \\ 0 \\ 0 \end{bmatrix} \mathbf{u}_s. \tag{2}$$

For the definition of symbols and variables the reader can refer to [15]. Model (2) is expressed in the primary reference frame, however, in order to illustrate the proposed FLC, it is useful to write the equations in the secondary flux reference frame, and it can be obtained by expressing the equations in a $x-y$ reference frame rotating with a speed equal to:

$$\omega_{mr} = \omega_r + \left(\frac{R_r}{L_{\sigma r}} - \frac{\hat{R}_r}{\hat{L}_m} \right) \frac{\psi_{mq}}{|\mathbf{\Psi}_r|} \tag{3}$$

with x-axis aligned with the $\mathbf{\Psi}_r$ space-vector. Thus, the final scalar equations are:

$$\frac{di_{sx}}{dt} = -a_{11} i_{sx} + a_{12}\psi_{mx} - a_{13}\psi_{rx} + \left(\omega_r + a_{31}\frac{\psi_{my}}{\psi_{rx}}\right) i_{sy} + \frac{u_{sx}}{L_{\sigma s}}, \tag{4a}$$

$$\frac{di_{sy}}{dt} = -\left(a_{11} + a_{31}\frac{\psi_{my}}{\psi_{rx}}\right) i_{sy} + a_{12}\psi_{my} - \omega_r i_{sx} + \frac{u_{sy}}{L_{\sigma s}}, \tag{4b}$$

$$\frac{d\psi_{mx}}{dt} = a_{21} i_{sx} - a_{22}\psi_{mx} + \omega_r \psi_{my} + a_{31}\frac{\psi_{my}^2}{\psi_{rx}} + a_{23}\psi_{ra}, \tag{4c}$$

$$\frac{d\psi_{my}}{dt} = a_{21} i_{sy} - a_{22}\psi_{my} - \omega_r \psi_{mx} + a_{31}\frac{\psi_{my}\psi_{mx}}{\psi_{rx}}, \tag{4d}$$

$$\frac{d\psi_{rx}}{dt} = a_{31}\psi_{mx} - a_{32}\psi_{rx}, \tag{4e}$$

where:

$$a_{11} = \frac{R_s + R_0}{L_{\sigma s}},\ a_{12} = \frac{R_0 L_r}{\hat{L}_m L_{\sigma s} L_{\sigma r}},\ a_{13} = \frac{R_0}{L_{\sigma s} L_{\sigma r}},\ a_{21} = R_0,$$

$$a_{22} = \frac{R_0 L_r}{\hat{L}_m L_{\sigma r}} + \frac{\hat{R}_r}{\hat{L}_m},\ a_{23} = \frac{R_0}{L_{\sigma r}},\ a_{31} = \frac{R_r}{L_{\sigma r}} - \frac{\hat{R}_r}{\hat{L}_m},\ a_{32} = \frac{R_r}{L_{\sigma r}}.$$

In model (4) it has been considered $\psi_{ry} = 0$, since its dynamic equation is $\frac{d\psi_{ry}}{dt} = -a_{32}\psi_{ry}$. This implies that ψ_{ry} converges to zero asymptotically independently of the operating conditions of the motor.

Finally, the mechanical equation of the motion of a LIM is:

$$M\frac{dv}{dt} = F - F_L, \tag{5}$$

where F is the net propulsive force generated by the LIM, F_L is the load force and M is the overall mass of the system (motor plus payload). Differently from the RIM case the net thrust is the algebraic sum of the electromagnetic propulsive force F_e (similar to the torque expression of the RIM) and the braking force due to the end effects F_{eb}. The expression of F_e and F_{eb} are:

$$F_e = \gamma M \psi_{rx} \psi_{my}, \tag{6a}$$

$$F_{eb} = \eta |\mathbf{\Psi}_m|, \tag{6b}$$

where $\gamma = \frac{3}{2}\frac{\pi p}{\tau_p L_{\sigma r} M}$ and $\eta = \frac{3}{2}\frac{\hat{L}_r}{\hat{L}_m^2}\frac{1-e^{-Q}}{\tau_m}$. Eqs. (6) provide the electromagnetic forces produced by the LIM, taking into consideration both the iron losses and the dynamic end effects, and provides important information. Indeed, the electromagnetic force of the a LIM is not obtained with the vector product between the secondary flux linkage and the primary current space-vectors, but the vector product of the secondary flux linkage and the three-phase magnetizing flux space-vectors. For further detail the reader is addressed to [15].

III. The FLC Considering the LIM Dynamic End-Effects and the iron losses

Looking at equations shown in the former Section, in particular those describing the speed and flux dynamics, it can be easily observed that they are not decoupled in each working condition, and even if the machine works at constant flux, there is a coupling due to the dependence of the parameters

on the speed. To overcome this problem, and obtain a fully decoupled linear model, a further feedback loop should be devised. With this aim, if two distinct controlled outputs are selected: ψ_{rx} and v, two distinct models can be proposed, i.e. the flux model and the speed model, using the feedback linearization method. The first model consists of the equations of the model described in the previous Section expressing the dynamics of the the flux along the x axis, ψ_{rx}. The other model consists of the equations expressing the dynamics of the mechanical speed v.

With regards to the flux model, it is possible to compute the Lie derivatives of ψ_{rx} up to the third order before the input u_{sx} appears in the equation. In particular, defining $x_{\psi 1} = \psi_{sx}$, $x_{\psi 2} = \dot{\psi}_{sx}$ and $x_{\psi 3} = \ddot{\psi}_{sx}$ the following equations can

$$\dot{x}_{\psi 1} = x_{\psi 2}, \qquad \dot{x}_{\psi 2} = x_{\psi 3}, \qquad \dot{x}_{\psi 3} = f_\psi + b_\psi u_{sx}. \tag{7}$$

where f_ψ is defined as follows:

$$\begin{aligned} f_\psi = {} & a_{31}a_{21}\left(-a_{11}i_{sx} + a_{12}\psi_{mx} - a_{13}\psi_{rx}\right) \\ & + \left(a_{31}a_{23} + a_{32}^2\right)\left(a_{31}\psi_{mx} - a_{32}\psi_{rx}\right) - a_{31}(a_{22} + a_{32}) \\ & \cdot \left(a_{21}i_{sx} - a_{22}\psi_{mx} + \omega_r\psi_{my} + a_{31}\frac{\psi_{my}^2}{\psi_{rx}} + a_{23}\psi_{rx}\right) \\ & + \frac{p\pi}{\tau_p}\left(a_{31}\gamma\psi_{my}^2\psi_{rx} - a_{31}\psi_{my}\frac{F_L}{M}\right) \\ & + a_{31}\omega_r\left(a_{21}i_{sy} - a_{22}\psi_{my} - \omega_r\psi_{mx} - a_{31}\frac{\psi_{mx}\psi_{my}}{\psi_{rx}}\right) \\ & - a_{31}^2\frac{\psi_{my}^2}{\psi_{rx}^2}\left(a_{31}\psi_{mx} - a_{32}\psi_{ra}\right) \\ & + 2a_{31}^2\frac{\psi_{my}}{\psi_{rx}}\left(a_{21}i_{sy} - a_{22}\psi_{my} - \omega_r\psi_{mx} - a_{31}\frac{\psi_{mx}\psi_{my}}{\psi_{rx}}\right). \end{aligned} \tag{8}$$

While b_ψ is defined as: $b_\psi = \frac{a_{31}a_{21}}{L_{\sigma s}}$.

With regards to the speed model, it is possible to compute the Lie derivatives of v up to the third order before that the input u_{sy} appears in the equation. In particular, defining $x_{v1} = v$, $x_{v2} = \dot{v}$ and $x_{v3} = \ddot{v}$ the following equations can be written:

$$\dot{x}_{v1} = x_{v2}, \qquad \dot{x}_{v2} = x_{v3}, \qquad \dot{x}_{v3} = f_v + b_v u_{sy}. \tag{9}$$

where f_v is defined as follows:

$$\begin{aligned} f_v = {} & \gamma\psi_{rx}a_{21}\left(-a_{11}i_{sy} + a_{12}\psi_{my} - \omega_r i_{sy} - a_{31}\frac{\psi_{my}i_{sy}}{\psi_{rx}}\right) \\ & + \gamma\left(a_{31}\psi_{mx} - a_{32}\psi_{rx}\right)\left(a_{21}i_{sy} - (a_{32} + a_{22})\psi_{my} - \omega_r\psi_{mx}\right) \\ & - \gamma\psi_{rx}(a_{32} + a_{22})\left(a_{21}i_{sy} - a_{22}\psi_{my} + \left(\omega_r + a_{31}\frac{\psi_{my}}{\psi_{rx}}\right)\psi_{mx}\right) \\ & - \gamma\psi_{rx}\left(\gamma\psi_{rx}\psi_{my} - \frac{F_L}{M}\right)\psi_{mx} \\ & - \gamma\psi_{rx}\omega_r\left(a_{21}i_{sx} - a_{22}\psi_{mx} + \omega_r\psi_{my} + a_{31}\frac{\psi_{my}^2}{\psi_{rx}} + a_{23}\psi_{rx}\right). \end{aligned} \tag{10}$$

While b_v is defined as: $b_v = \frac{\gamma a_{21}\psi_{rx}}{L_{\sigma s}}$.

Note that for both models (7) and (9), in order to reduce the computational load of the controller, the derivatives of the parameter with respect to the speed are been assumed zero, which is an absolutely reasonable approximation.

Models (7) and (9) show that the flux and speed models have the same structure (but with different dimensions). Moreover, choosing the control variables as follows:

$$u_{sx} = \frac{1}{b_\psi}\left(-f_\psi + \nu_x\right), \qquad u_{sy} = \frac{1}{b_v}\left(-f_v + \nu_y\right), \tag{11}$$

models (7) and (9) becomes two chains of integrators as follows:

$$\dot{x}_{\psi 1} = x_{\psi 2}, \qquad \dot{x}_{\psi 2} = x_{\psi 3}, \qquad \dot{x}_{\psi 3} = \nu_x. \tag{12}$$

$$\dot{x}_{v1} = x_{v2}, \qquad \dot{x}_{v2} = x_{v3}, \qquad \dot{x}_{v3} = \nu_y. \tag{13}$$

Therefore ν_x and ν_y can be designed by using classical tools for linear systems to satisfy design requirements for linear models (12) and (13).

In summary to achieve the input-output feedback linearizing control of LIM, considering both the end effects and the iron losses, the inputs ν_x and ν_y have to be selected through a first state feedback in order to fix the flux and speed dynamics. Then, through a second state feedback, the voltage source u_{sx} and u_{sy} are obtained starting from ν_x and ν_y by means of (11). Note that the only condition to ensure the existence of this feedback is that the flux $|\psi_{rx}|$ is different from zero. Finally, it is useful to note that the linearization terms (8) and (10) have never been shown in literature, and they have been obtained specifically in this work to account for both end effects and iron losses.

The block diagram of the feedback control scheme of the LIM drive is represented in Fig. 1.

A. Design of flux and speed controllers

In order to make ψ_r and v track the references ψ_{ref} and v_{ref}, the input signals ν_x and ν_y are designed as:

$$\begin{aligned} \nu_x = {} & -k_{\psi 1}\left(x_{\psi 1} - \psi_{ref}\right) - k_{\psi 2}\left(x_{\psi 2} - \frac{d\psi_{ref}}{dt}\right) \\ & - k_{\psi 3}\left(x_{\psi 3} - \frac{d^2\psi_{ref}}{dt^2}\right) + \frac{d^3\psi_{ref}}{dt^3}, \end{aligned} \tag{14}$$

$$\begin{aligned} \nu_y = {} & -k_{v1}\left(x_{v1} - v_{ref}\right) - k_{v2}\left(x_{v2} - \frac{dv_{ref}}{dt}\right) \\ & - k_{v3}\left(x_{v3} - \frac{d^2v_{ref}}{dt^2}\right) + \frac{d^3v_{ref}}{dt^3}, \end{aligned} \tag{15}$$

where $k_{\psi 1}$, $k_{\psi 2}$, $k_{\psi 3}$, k_{v1} and k_{v2} are positive constant design parameters. These are determined in order to impose an exponentially stable dynamic of the decoupled, linear, time-invariant, systems constituted by the flux and speed errors $e_{\psi_r} = \psi_r - \psi_{ref}$ and $e_v = v - v_{ref}$:

$$\frac{d^3e_{\psi_r}}{dt^3} = -k_{\psi 1}e_{\psi_r} - k_{\psi 2}\frac{de_{\psi_r}}{dt} - k_{\psi 3}\frac{d^2e_{\psi_r}}{dt^2}, \tag{16}$$

$$\frac{d^2e_v}{dt^2} = -k_{v1}e_v - k_{v2}\frac{de_v}{dt} - k_{v3}\frac{d^2e_v}{dt^2}. \tag{17}$$

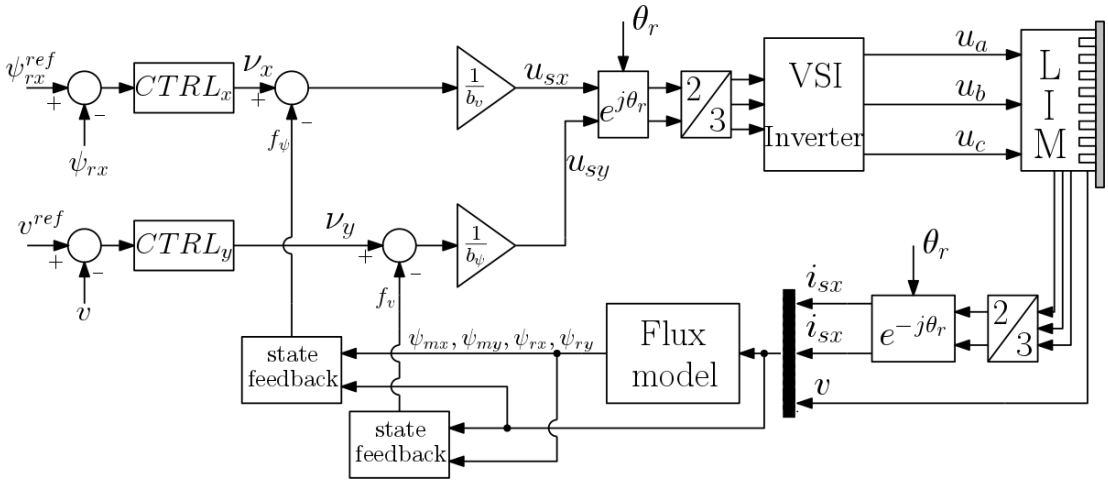

Figure 1. Block diagram of the proposed control scheme of the LIM drive .

In particular, it is possible to assign both flux and speed dynamics by choosing suitably the zeros of the following characteristic polynomials:

$$\Delta_\psi(\lambda) = k_{\psi 1} + k_{\psi 2}\lambda + k_{\psi 3}\lambda^2 + \lambda^3, \tag{18}$$

$$\Delta_v(\lambda) = k_{v1} + k_{v2}\lambda + k_{v3}\lambda^2 + \lambda^3. \tag{19}$$

In this case, the parameters have been determined assuming that the desired zeros are $\lambda_1 = -\zeta\omega_n + j\omega_n\sqrt{1-\zeta^2}$, $\lambda_2 = -\zeta\omega_n - j\omega_n\sqrt{1-\zeta^2}$ and $\lambda_3 = \sigma$, where ω_n and ζ are the natural frequency and the damping factor respectively, while σ is a negative real number. This choice ensures an exponentially stable error dynamics. Moreover, for the speed controller, the following values have been assumed $\omega_n = 100$, $\xi = 0.9$ and $\sigma = -400$, while for the flux controller, the following values have been assumed $\omega_n = 150$, $\xi = 0.9$ and $\sigma = -400$.

IV. Test Set-up

A test set-up has been suitably built to experimentally verify the goodness of the proposed input-output feedback linearization technique considering both the end-effects and the iron losses. The LIM under test is a Baldor LMAC1607C23D99, whose rated data and electrical parameters are shown in Table I. The LIM has been equipped with a linear encoder Numerik Jena LIA series, and it presents a secondary track of length 1.6 m. Fig. 2 shows a photograph of the test set-up. The employed test set-up consists of:

- A three-phase linear induction motor, whose parameters are shown in Fig. 2.b;
- A frequency converter composed of a three-phase diode rectifier and a 7.5 kVA three-phase VSI;
- A dSPACE card (DS1103) with a PowerPC 604e running at 400 MHz and a floating-point DSP TMS320F240.

The test set-up is also equipped with a torque-controlled Permanent Magnets Synchronous Motor (*PMSM*) model Emerson Unimotor HD 067UDB305BACRA, which is mechanically coupled to the LIM by a pulley-strap system to behave as an active load for the LIM.

Figure 2. Photograph of the LIM experimental set-up.

Table I
Parameters of the LIM model

Symbols	Values
Rated power (W)	425
Rated voltage (V)	380
Rated frequency (Hz)	60
Pole-pairs	3
Rated speed (m/s)	6.85
Rated thrust (N)	200
Mass (kg)	20
Inductor resistance R_s (Ω)	11
Inductor inductance L_s (mH)	634
Induced part resistance R_r (Ω)	32.6
induced part inductance L_r (mH)	758
3-phase magnetizing inductance L_m (mH)	517

V. Experimental Results

The proposed input-output feedback linearization control has been experimentally tested on the above-described test set-up. Because of the limited length of the secondary track (1.6 m), the experimental test has been performed at low speed, 0.4 m/s (about 6% of the rated speed). Two experimental tests have been performed.

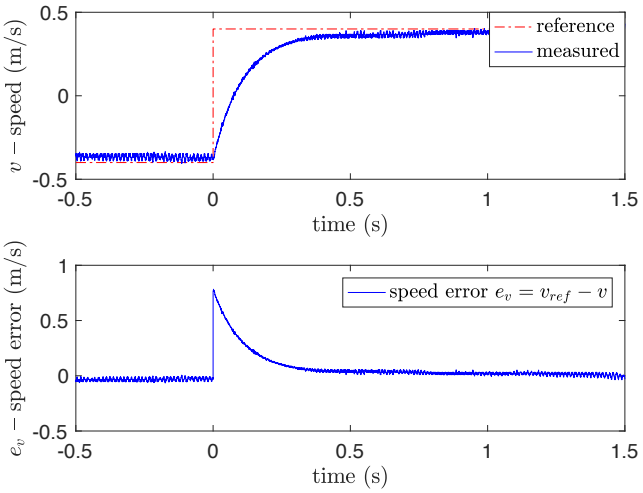

Figure 3. Reference and measured speed during a speed reversal from -0.4 to 0.4 m/s.

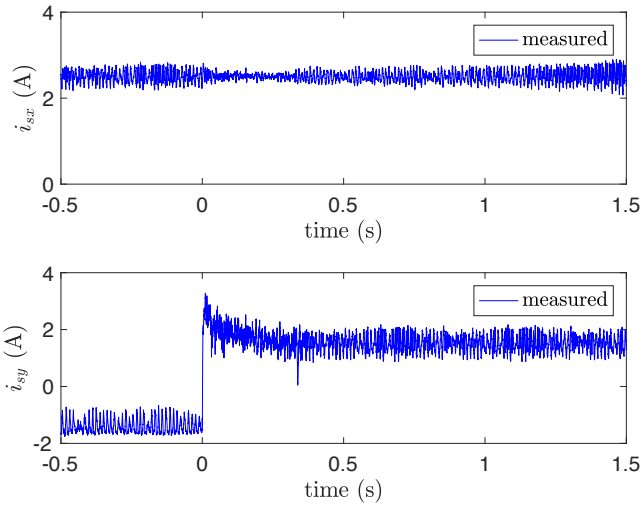

Figure 4. Direct and quadrature primary current components i_{sx} and i_{sy} during a speed reversal from -0.4 to 0.4 m/s.

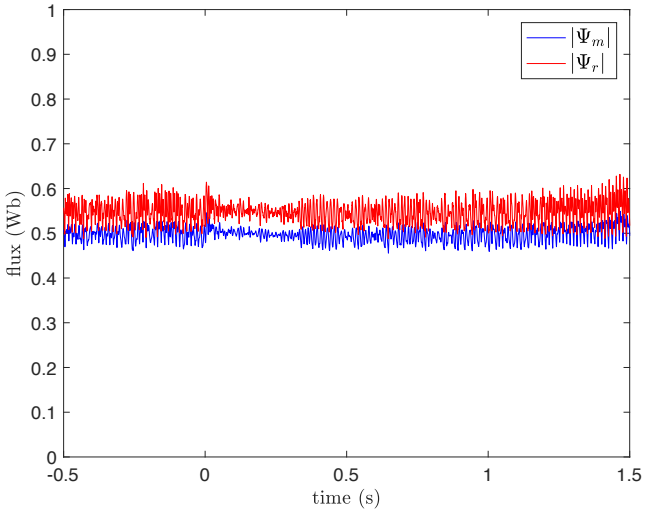

Figure 5. Secondary $|\Psi_r|$ and three-phase magnetizing $|\Psi_m|$ flux amplitudes during a speed reversal from -0.4 to 0.4 m/s.

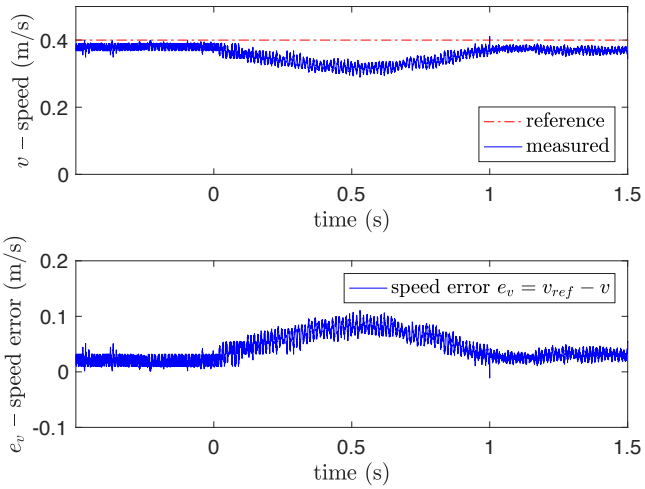

Figure 6. Reference and measured speed during a load step insertion and release of 30 N at constant speed of 0.4 m/s.

In the first test, the LIM drive has been commanded a speed reversal from -0.4 to 0.4 m/s at no-load. Fig. 3 shows the reference and measured speed obtained with the proposed FLC during this test, as well as the corresponding speed tracking error. It can be observed that the FLC works properly, ensuring high performance in speed control, with the entire reversal accomplished in less than 0.4 s and the speed tracking error converging to zero in the same time interval. Correspondingly, Fig. 4 shows the direct and quadrature components of the primary currents expressed in the secondary flux (field) reference frame during the same test. It can be observed that, while i_{sx} is commanded to a constant value accounting for a constant magnetization level of the LIM, i_{sy} presents a stepwise waveform with a peak occurring during the speed transient and a steady-state value covering the friction force of the LIM (very high in the LIM under test). Fig. 5 shows the corresponding values of the Secondary $|\Psi_r|$ and three-phase magnetizing $|\Psi_m|$ flux amplitudes. It can be observed that the control system maintains both flux amplitudes at a constant value, consistently with the current waveforms, since the difference between the two is caused by the presence of the friction load force.

In the second test, the LIM drive has been operated at the constant speed of 0.4 m/s. A load force step of amplitude of 30 N has been firstly applied and then released. Figs. 6, 7 and 8 show the same kind of waveforms, like test 1. The speed waveforms show that the FLC is able to cover the load step application and release, with the measured speed firstly reducing with respect to the reference and then approaching towards it again, as expected. The current waveforms, consistently, show that i_{sx} is commanded to a constant value accounting for a constant magnetization level of the LIM,

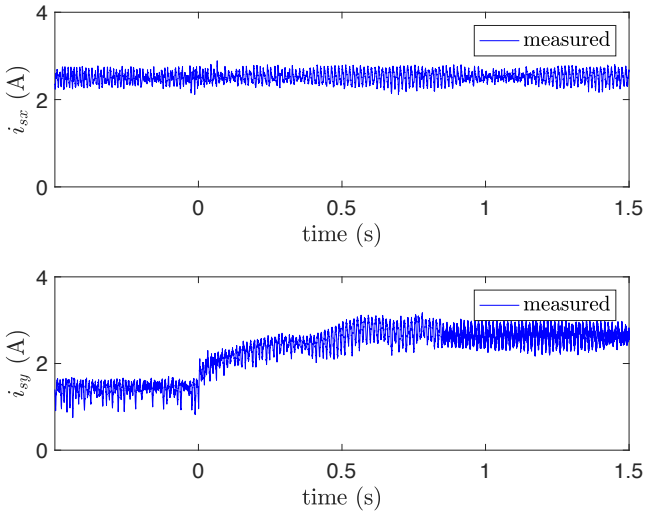

Figure 7. Direct and quadrature primary current components i_{sx} and i_{sy} during a load step insertion and release of 30 N at constant speed of 0.4 m/s.

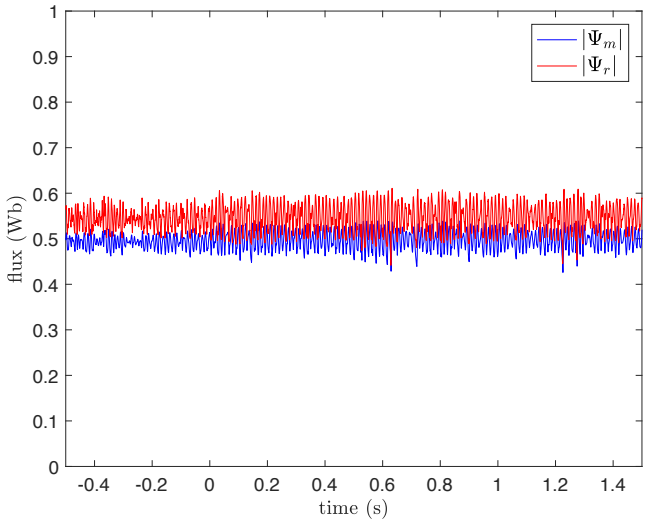

Figure 8. Secondary $|\Psi_r|$ and three-phase magnetizing $|\Psi_m|$ flux amplitudes during a load step insertion and release of 30 N at constant speed of 0.4 m/s.

and i_{sy} presents a stepwise shape accounting for the load force compensation. Finally, the flux waveforms show that the control system maintains both flux amplitudes at a constant value, in consistence with the current waveforms.

VI. Conclusion

This paper proposes a new input-output feedback linearization control technique of LIMs taking into consideration both the dynamic end-effects and the iron losses. Starting from a previously conceived dynamic model including both the dynamic end-effects and the iron losses, all the theoretical framework of the FLC has been developed. The proposed FLC improves a previously proposed version of FLC, since it considers also the iron losses, which play a more important role in the LIM than in the RIM. The proposed FLC has been experimentally tested on a suitably developed test set-up.

References

[1] E. R. Laithwaite, "Linear electric machines – a personal view," *Proceedings of the IEEE*, vol. 63, no. 2, pp. 250–290, 1975.

[2] S. Yamamura, "Theory of linear induction motors," *New York, Halsted Press, 1979. 246 p.*, vol. 1, 1979.

[3] S. A. Nasar and I. Boldea, *Linear electric motors: theory, design, and practical application*. Prentice-Hall inc., 1987.

[4] W. Xu, M. R. Islam, and M. Pucci, *Advanced Linear Machines and Drive Systems*. Springer, 2019.

[5] G. Gentile, N. Rotondale, and M. Scarano, "Analisi del funzionamento transitorio del motore lineare," *L'Energia elettrica*, no. 5, 1987.

[6] ——, "The linear induction motor in transient operation," *L'Energia Elettrica*, no. 7-8, 1988.

[7] W. Xu, J. G. Zhu, Y. Zhang, Z. Li, Y. Li, Y. Wang, Y. Guo, and Y. Li, "Equivalent circuits for single-sided linear induction motors," *IEEE Transactions on Industry Applications*, vol. 46, no. 6, pp. 2410–2423, 2010.

[8] M. Pucci, "State space-vector model of linear induction motors," *Industry Applications, IEEE Transactions on*, vol. 50, no. 1, pp. 195–207, 2014.

[9] F. Alonge, M. Cirrincione, M. Pucci, and A. Sferlazza, "Input-output feedback linearizing control of linear induction motor taking into consideration the end-effects. Part I: Theoretical analysis," *Control Engineering Practice*, vol. 36, pp. 133–141, 2015.

[10] ——, "Input–output feedback linearization control with on-line MRAS-based inductor resistance estimation of linear induction motors including the dynamic end effects," *IEEE Transactions on Industry Applications*, vol. 52, no. 1, pp. 254–266, 2016.

[11] F. Alonge, M. Cirrincione, F. D'ippolito, M. Pucci, and A. Sferlazza, "Adaptive feedback linearizing control of linear induction motor considering the end-effects," *Control Engineering Practice*, vol. 55, pp. 116–126, 2016.

[12] F. Alonge, M. Cirrincione, F. D'Ippolito, M. Pucci, and A. Sferlazza, "Active disturbance rejection control of linear induction motor," *IEEE Transactions on Industry Applications*, vol. 53, no. 5, pp. 4460–4471, 2017.

[13] M. Cirrincione, A. Accetta, M. Pucci, and G. Vitale, "MRAS speed observer for high-performance linear induction motor drives based on linear neural networks," *IEEE transactions on Power Electronics*, vol. 28, no. 1, pp. 123–134, 2012.

[14] A. Accetta, M. Cirrincione, M. Pucci, and G. Vitale, "Neural sensorless control of linear induction motors by a full-order Luenberger observer considering the end effects," *IEEE Transactions on Industry Applications*, vol. 50, no. 3, pp. 1891–1904, 2013.

[15] A. Accetta, M. Cirrincione, M. Pucci, and A. Sferlazza, "State space-vector model of linear induction motors including iron losses part I: Theoretical analysis," *IEEE Transactions on Industry Applications*, vol. 56, no. 1, pp. 235–244, 2020.